

Momentum-dependent light scattering in a 2D Heisenberg antiferromagnet

A. Donkov and A. V. Chubukov

Department of Physics, University of Wisconsin, Madison, WI 53706, USA

(Dated: October 9, 2018)

Motivated by the achievements of the X-ray scattering technique, we analyzed the profile of the light scattering intensity $R(q, \omega)$ at a finite q in a 2D Heisenberg antiferromagnet. Previous Raman scattering studies at $q = 0$ identified the two-magnon peak in B_{1g} scattering geometry. We found that the B_{1g} peak disperses downwards at a finite q , and its intensity increases, reaching its maximum at $q = q_0 = (0, \pi)$ and symmetry related points. In addition, the intensity in the A_{1g} geometry becomes non-zero at a finite q , and also displays a two-magnon peak which gains strength and disperses to larger frequencies with increasing q , and reaches its highest intensity at q_0 . We found that the profile of $R(q_0, \omega)$ is equivalent in A_{1g} and B_{1g} geometries.

PACS numbers: 78.70.Ck, 72.10.Di, 78.30.-j, 75.30.Ds

Raman scattering is a powerful probe of magnetic and electronic correlations in interacting electron systems. Raman studies of antiferromagnetic parent compounds of the cuprates in early 90's provided the first estimates of the Heisenberg exchange integrals in La_2CuO_4 and $YB_2C_3O_6$. The values of $J \sim 120 - 140 meV$ were extracted from the positions of the B_{1g} two-magnon peak which, according to the theory, are located at approximately $2.7J$ [1]. The values of J extracted from the Raman studies were later confirmed by neutron scattering measurements [2].

The traditional framework for the understanding of the two-magnon Raman scattering in antiferromagnets has been the semi-phenomenological Loudon-Fleury model for the interaction of light with spin degrees of freedom [3]. The model assumes the existence of the matrix element M_R for the direct process in which incident photon with energy ω_i comes in, an outgoing photon with energy ω_f comes out, and two magnons are excited with energies $\Omega(k_1)$ and $\Omega(k_2)$ (see Fig. 1). The energy conservation implies $\Omega(k_1) + \Omega(k_2) = \hbar(\omega_i - \omega_f) = \hbar\omega$. The transferred frequency ω is usually order of magnitude smaller than $\omega_{i,f}$.

Quite generally, the matrix element M_R depends on the two frequencies ω_i and ω_f , the two momenta, either of two photons or two magnons, and on the polarizations $\hat{\mathbf{e}}_i$ and $\hat{\mathbf{e}}_f$ of the incoming and outgoing light. For the two most frequently studied cases of A_{1g} and B_{1g} scattering, the polarizations are $\hat{\mathbf{e}}_i = (\hat{\mathbf{x}} + \hat{\mathbf{y}})/\sqrt{2}$, $\hat{\mathbf{e}}_f = (\hat{\mathbf{x}} + \hat{\mathbf{y}})/\sqrt{2}$, for A_{1g} scattering, and $\hat{\mathbf{e}}_i = (\hat{\mathbf{x}} + \hat{\mathbf{y}})/\sqrt{2}$, $\hat{\mathbf{e}}_f = (\hat{\mathbf{x}} - \hat{\mathbf{y}})/\sqrt{2}$, for B_{1g} scattering. For non-resonant scattering, which we consider, the frequency dependence of M_R only affects the overall factor, and the interesting physics comes from the momentum dependence of M_R . The two magnon momenta can be parameterized as $k_1 = k + q/2$, $k_2 = -k + q/2$, where q is the transferred photon momentum, then $M_R = M_R(k, q)$. At $q = 0$, $M_R \propto \cos k_x + \cos k_y$ in A_{1g} geometry, and $M_R \propto \cos k_x - \cos k_y$ in B_{1g} geometry.

Without the final state interaction, the intensity of the absorption of light $R_0(q, \omega)$ is obtained from the Fermi

golden rule, and is given by

$$R_0(q, \omega) \propto \sum_k M_R^2(k, q) \times \delta[\hbar\omega - (\Omega(k + q/2) + \Omega(-k + q/2))]. \quad (1)$$

Below we label by $R(q, \omega)$ the full intensity, which includes the final state interaction.

In Raman scattering experiments with visible light, typical frequencies of the incident light are $\omega_{i,f}/(2\pi) \sim 510^{14}$ Hz, and the corresponding wave-vectors $q_{i,f} \sim 1.510^7$ m⁻¹. Typical momenta k for magnons near magnetic Brillouin zone boundary, which mostly contribute to Raman scattering, are of the order π/d , where $d \sim 10^{-10}$ m is the lattice constant. Accordingly, $k \sim 10^{10}$ m⁻¹, three orders of magnitude larger than $q_{i,f}$, in which case one can safely set $q = 0$ in Eq. (1) [4]. The approximation $R(q, \omega) \approx R(q = 0, \omega)$ has been used in all previous calculations of the Raman intensity [5, 6, 7].

In recent years, however, a new resonant inelastic X-ray scattering technique (RIXT) has been developed, which allows one to probe the intensity $R(q, \omega)$ at a finite q [8, 9, 10]. The frequencies of X rays are tuned to the energies of atomic transitions and are several orders of magnitude larger than for conventional Raman experiments: $\omega_i/(2\pi) \sim 210^{18}$ Hz, [11]. The corresponding momenta are then $q_{i,f} \sim 610^{10}$ m⁻¹. These momenta are comparable to the typical magnon momenta k . As a result, RIXT technique allows one to measure the light intensity $R(q, \omega)$ at a finite q .

A RIXT study of the undoped and weakly doped $La_{2-x}Sr_xCuO_4$ and undoped Nd_2CuO_4 has recently been carried out by Hill et al [10]. In both undoped compounds, the authors scanned various momenta q , and at $q = q_0 = (0, \pi)$ observed a sharp peak in $R(q_0, \omega)$ at $500 meV$. On deviations from q_0 , the peak moves to smaller frequencies and broadens. The doping dependence of the peak at q_0 is similar to that of the two-magnon Raman peak – both broaden with doping and disappear near optimal doping. Based on this similarity, the authors of [10] argued that the peak at q_0 is likely a two-magnon feature at a finite q . This is corroborated by the fact that the density of states (DOS)

of two non-interacting magnons has a peak at $(0, \pi)$ at $3.5J \sim 500meV$.

The presence of the peak in the DOS, however, does not necessarily imply the peak in $R_0(q_0, \omega)$ as the matrix element M_R may counterweight the DOS effect. Besides, magnons do interact in the final state, and this interaction may substantially affect the profile of $R(q, \omega)$ compared to that of $R_0(q, \omega)$.

In this communication, we analyze $R(q, \omega)$ in A_{1g} and B_{1g} geometries in two-dimensional (2D) antiferromagnetic Mott insulators (e.g., parent compounds of high-temperature superconductors). Like we said above, at $q = 0$, the Raman response in the B_{1g} geometry contains the two-magnon peak at $\omega \approx 2.7J$. In A_{1g} geometry the Raman intensity vanishes at $q = 0$ because Loudon-Fleury and Heisenberg Hamiltonians commute [5, 6]. We consider how both features are modified at a finite q . We show that the position of the two-magnon peak in the B_{1g} geometry evolves with q , and at q_0 the peak is located at $2.4J \sim 340meV$. We show that the intensity of the B_{1g} peak actually increases at a finite q and is the largest at q_0 and symmetry-related points. We further show that in A_{1g} geometry, $R(q, \omega)$ is non-zero at a finite q , and the intensity is again the largest at q_0 . We found that for $q = q_0$, the intensities $R(q, \omega)$ in A_{1g} and B_{1g} channels are equivalent both with and without final state interaction.

Our results cannot be directly applied to the experiments by Hill et al [10] as they found the peak at q_0 in the geometry when the incident polarization is along c -axis. To obtain the matrix element in such geometry one would need to consider hopping between 2D planes. At the same time, our A_{1g} and B_{1g} results show that the profile of the peak in $R(q_0, \omega)$ is predominantly determined by the interplay between the two-magnon DOS and magnon-magnon interaction, while the momentum dependence of the matrix element M_R does not play a substantial role near q_0 . We therefore expect that the (identical) profile of $R(q_0, \omega)$ in A_{1g} and B_{1g} geometry is similar to that for c -axis polarization of the light, and the intensity is just stronger in c -axis geometry.

The derivation of the matrix element M_R for x -ray scattering which involves high-energy photons in general requires a careful consideration of core atomic transitions [10, 13]. The outcome of this consideration is some effective direct coupling between x -rays and two magnons. In the following, we adopt an approach borrowed from Raman studies and derive the Raman matrix element by the same method as in Ref. [5], which we extended to finite q . Namely, we depart from the 2D half-filled Hubbard model with strong on-site repulsion U and the nearest-neighbor hopping t , expand the hopping term in vector potential \mathbf{A} , and restrict with the on-site interaction term $\mathcal{H}_{int} = -(e/\hbar c) \sum_q \mathbf{j}_q \mathbf{A}_{-q}$ between the vector potential and the fermionic current. We then introduce antiferromagnetic long-range order parameter Δ ($\approx U/2$ at $U \gg t$ which we only consider), and split quasiparticles into conduction and valence bands, with energies

$\pm \sqrt{\Delta^2 + \epsilon_k^2}$, where $\epsilon_k = -2t(\cos k_x + \cos k_y)$. We then obtain from the model the interaction vertices between magnons and conduction and valence fermions. At large U/t , the dominant interactions are the ones in which fermion flips from the conduction to the valence band and vice versa after emitting a magnon. To keep calculations under control, we extended the model to “large S ” by introducing $2S$ fermionic flavors [12]. For large S , the corrections to our vertices are small, of order $1/S$.

Like we just said, for energies of the incident phonons well above Hubbard U , the matrix element M_R comes from the core level atomic transitions rather than from the excitations across the Hubbard gap. Still, we believe that the derivation using “Raman technique” is useful as it shows the difference between the conventional Raman scattering with $q = 0$ and a finite q scattering in different scattering geometries. Besides, as we will see, for scattering near $(0, \pi)$ the profile of $R(q, \omega)$ is determined predominantly by the structure of the DOS and magnon-magnon interaction, while the matrix element M_R can be safely set to be a constant. This implies that the results below could be obtained with just a phenomenological M_R .

The processes which contribute to the matrix element M_R in finite q Raman scattering are the ones in which incident light creates a particle-hole pair, which creates two magnons, either from two different lines in the particle-hole bubble, or from the same line, and then annihilates into outgoing light. The corresponding two diagrams are presented in Fig. 1. [The diagram b has a “parasitic” contribution which for $q = 0$ is canceled out by the additional diagram with an extra fermion-fermion interaction [5]. We verified that the same cancellation occurs also at a finite q]. Evaluating the two diagrams and adding them up, we obtain the matrix element in various geometries in the form

$$M_R(k, q) = -8t^2 \left[\frac{2\Delta}{4\Delta^2 - \omega_i^2} \right] \times \\ \{ [\hat{\mathbf{e}}_{ix} \hat{\mathbf{e}}_{fx}^* \cos(q_x/2) + \hat{\mathbf{e}}_{iy} \hat{\mathbf{e}}_{fy}^* \cos(q_y/2)] (\lambda_{k+q/2} \mu_{-k+q/2} + \\ + \lambda_{-k+q/2} \mu_{k+q/2}) - [\hat{\mathbf{e}}_{ix} \hat{\mathbf{e}}_{fx}^* \cos(k_x) + \hat{\mathbf{e}}_{iy} \hat{\mathbf{e}}_{fy}^* \cos(k_y)] \times \\ \times (\mu_{k+q/2} \mu_{-k+q/2} + \lambda_{k+q/2} \lambda_{-k+q/2}) \}, \quad (2)$$

where $\mu_k = \frac{1}{\sqrt{2}} \sqrt{\frac{1}{\sqrt{1-\gamma_k^2}} + 1}$, $\lambda_k = \frac{\gamma_k}{|\gamma_k| \sqrt{2}} \sqrt{\frac{1}{\sqrt{1-\gamma_k^2}} - 1}$, and $\gamma_k = (\cos(k_x) + \cos(k_y))/2$. The magnon energy Ω_k is given by $\Omega_k = E_{max} \sqrt{1 - \gamma_k^2}$, where $E_{max} = 4JS (= 2J)$, and $J = t^2/4U$. At $q = 0$, the expression in Eq. (2) coincides with that in earlier works [5, 6]. In particular, one can easily verify that $M_R(k, 0)$ vanishes in A_{1g} geometry. At $q \neq 0$, the matrix element is non-zero in all scattering geometries, including A_{1g} . Furthermore, a simple trigonometric analysis shows that at $q = q_0 = (0, \pi)$,

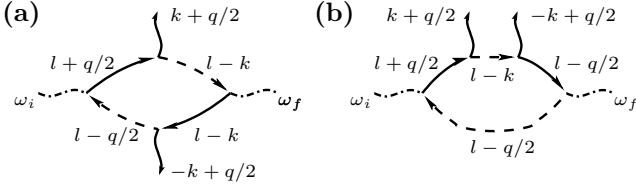


FIG. 1: The diagrams for the Raman matrix element $M_R(k, q)$. Solid and dashed lines represent conduction and valence electrons. The dash-dotted lines represent incoming and outgoing photons, and the solid wavy lines represent magnons. The full set includes an extra diagram (not shown) which cancels out a parasitic contribution from the diagram b, see [5].

the values of $M_R(k, q_0)$ in B_{1g} and A_{1g} geometries are identical.

Without final state interaction, the scattering intensity $R_0(q, \omega)$ is given by Eq. (1). In the top panels of Fig. 2, 3, we present the results for $R_0(q, \omega)$ for A_{1g} and B_{1g} scattering. We see that in A_{1g} geometry, the two-magnon peak gradually emerges as q increases, and progressively shifts to larger frequencies. In B_{1g} geometry, the largest intensity without final state interaction is still at $q = 0$. At a finite q , the peak position shifts to lower frequencies. In Fig. 4, top panel, we present the profile of $R_0(q_0, \omega)$ (a dashed line) which, we remind, is identical in A_{1g} and B_{1g} geometries. We see that $R_0(q_0, \omega)$ has a sharp peak at $\omega = \sqrt{3}E_{max}$ followed by the shoulder at $\omega = 2E_{max}$, which is the maximum value of the energy of two magnons. The position of the peak at $\sqrt{3}E_{max}$ can be traced back to the behavior of $\delta[\omega - (\Omega(k + q_0/2) + \Omega(k - q_0/2))]$, as $\Omega(k + q_0/2) + \Omega(k - q_0/2)$ has an extended van-Hove singularity at the set of k -points for which $\Omega(k_0 + q_0/2) + \Omega(k_0 - q_0/2) = \sqrt{3}E_{max}$ (see the bottom panel of Fig. 4). The Raman matrix element $M(k, q_0)$ is regular and we found that its k -dependence only weakly affects the form of $R_0(q_0, \omega)$.

The Fermi golden-rule results for $R_0(q, \omega)$ are of limited use, however, as two excited magnons interact in the final state. The magnon-magnon interaction is not small for $S = 1/2$, and in general substantially affects the scattering profile. We obtained the vertex for magnon-magnon interaction by a standard technique: we used the fact that the half-filled Hubbard model at large U reduces to the Heisenberg 2D antiferromagnet with nearest neighbor exchange, $H = J \sum_{\langle i, j \rangle} S_i \cdot S_j$, re-expressed spin operators in terms of Holstein-Primakoff bosons α and β which describe excitations in the two sublattices, and restricted with only the interaction term $\alpha^\dagger \beta^\dagger \alpha \beta$ which describes multiple scattering of two excited magnons. This procedure is similar to the one used in previous works (see, e.g., [5, 14]), the new element is that now the total momentum of the two magnons is non-zero. The relevant interaction part of the Heisenberg Hamiltonian is

$$H' = \sum_k' \sum_l' \Gamma_q(k, l) \alpha_{k+q/2}^\dagger \beta_{-k+q/2}^\dagger \beta_{-l+q/2} \alpha_{l+q/2},$$

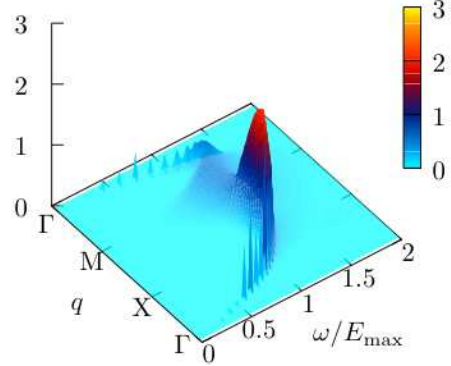
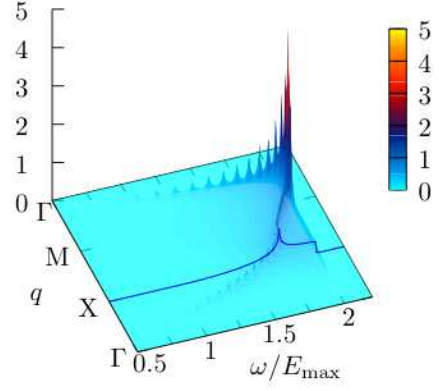


FIG. 2: The scattering intensity in the A_{1g} geometry along $\Gamma - X - M - \Gamma$ direction, where $\Gamma = (0, 0)$, $X = (\pi, \pi)$, and $M = (0, \pi)$. Top panel, without final state magnon-magnon interaction. Bottom panel - with the final state interaction. The largest intensity for the full $R(q, \omega)$ is at $q_0 = (0, \pi)$.

where the primes indicate that the summation is over the magnetic Brillouin zone, and

$$\begin{aligned} \Gamma_q(k, l) = & -\frac{8J}{N} \times \{ \\ & \gamma_{k-l} (\mu_{k+q/2} \mu_{l+q/2} \mu_{-k+q/2} \mu_{-l+q/2} + (\mu \leftrightarrow \lambda)) \\ & + \gamma_q (\mu_{k+q/2} \lambda_{l+q/2} \lambda_{-k+q/2} \mu_{-l+q/2} + (\mu \leftrightarrow \lambda)) \\ & - \frac{1}{2} [\gamma_{-k+q/2} (\mu_{k+q/2} \mu_{l+q/2} \mu_{-k+q/2} \lambda_{-l+q/2} + (\mu \leftrightarrow \lambda)) \\ & + \gamma_{-l+q/2} (\mu_{k+q/2} \mu_{l+q/2} \lambda_{-k+q/2} \mu_{-l+q/2} + (\mu \leftrightarrow \lambda)) \\ & + \gamma_{k+q/2} (\mu_{k+q/2} \lambda_{l+q/2} \mu_{-k+q/2} \mu_{-l+q/2} + (\mu \leftrightarrow \lambda)) \\ & + \gamma_{l+q/2} (\lambda_{k+q/2} \mu_{l+q/2} \mu_{-k+q/2} \mu_{-l+q/2} + (\mu \leftrightarrow \lambda))] \}. \end{aligned}$$

We computed the renormalization due to magnon-magnon interaction in the RPA approximation, by projecting the interaction onto $M_R(k, q)$ for different geometries, i.e., by approximating $\Gamma_q(k, l)$ by $B_q M_R(k, q) M_R(l, q)$, where $B_q = \sum_{k, l}' \Gamma_q(k, l) M_R(k, q) M_R(l, q) / (\sum_k' M_R^2(k, q))^2$. In this approximation, the total scattering intensity

$$R(q, \omega) \propto \text{Im} \frac{R_0(q, \omega)}{1 - B R_0(q, \omega)}, \quad (3)$$

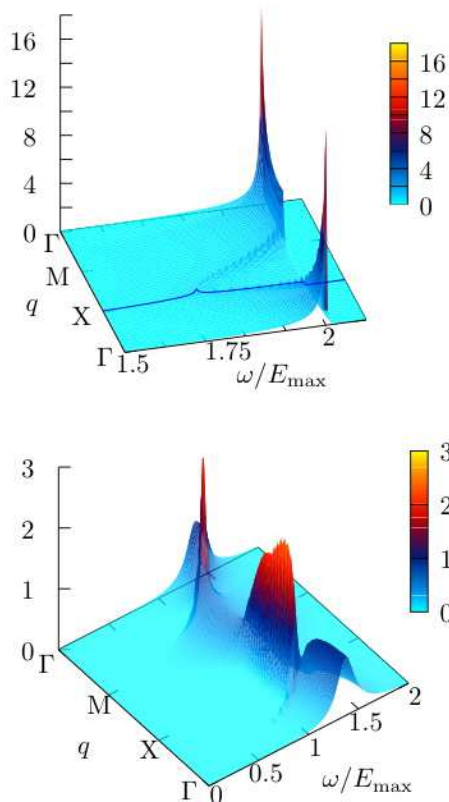


FIG. 3: Same as in Fig.2, but for B_{1g} geometry. The intensity for the full $R(q, \omega)$ is again the largest for $q_0 = (0, \pi)$.

where

$$R_0(q, \omega) = \sum_k' \frac{|M_R(k, q)|^2}{\omega - (\Omega_{k+q/2} + \Omega_{-k+q/2}) + i\delta}.$$

We set $S = 1/2$ at the end of calculations. For q near $q_0 = (0, \pi)$, we obtained $B \approx -3$, i.e., the final state interaction is quite important.

The results for the scattering intensity $R(q, \omega)$ renormalized by the final state magnon-magnon interaction are presented in the bottom panels of Fig. 2, 3. We see that both A_{1g} and B_{1g} scattering are substantially sharpened up around $q = q_0$, where the intensity is still at maximum in both geometries.

We verified that the final state interaction does not break the equivalence between the scattering intensities in A_{1g} and B_{1g} geometries right at q_0 . In Fig. 4, top panel, we plot the full intensity $R(q_0, \omega)$ versus frequency (a solid line). Comparing this result with $R_0(q, \omega)$ (a dashed line on the same figure), we see that after the final state interaction, the peak gets sharper and more symmetric, and also shifts to a lower frequency, about $1.2E_{max}$. *That the fully renormalized intensity $R(q, \omega)$ has a sharp maximum at q_0 is the central result of our paper.*

The final state magnon-magnon interaction at a finite q was earlier analyzed by Lorenzana and Sawatzky [16]

in the study of phonon-assisted optical absorption. In their case, a finite momentum q of two magnons is equivalent to a phonon momentum. Their effective matrix element for two-magnon vertex is different from ours and belongs to two-dimensional representation of the tetragonal group D_{4h} . Still, our results are very similar to theirs – they also found that magnon-magnon interaction gives rise to a sharp peak in the absorption near $1.2E_{max}$. The only distinction between our results and their is that in their case the peak moves to higher frequencies on moving from q_0 towards $(0, 0)$, while we found that A_{1g} peak moves to smaller frequencies, and B_{1g} peak position remains almost unchanged

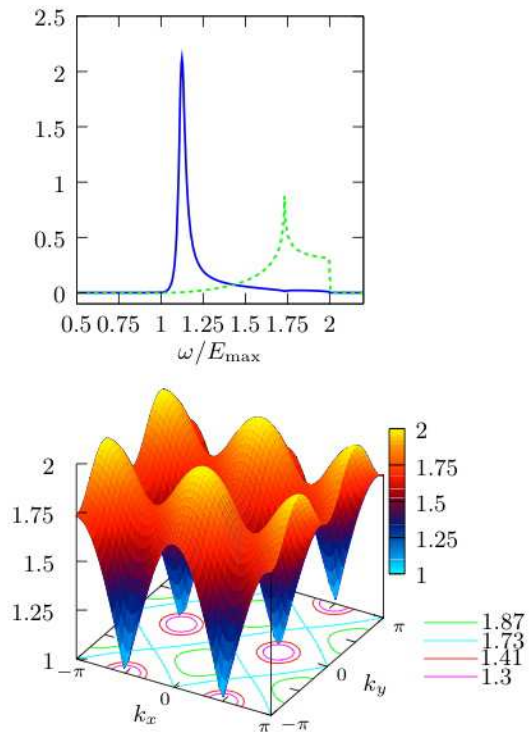


FIG. 4: Top panel: the scattering intensities at $q_0 = (0, \pi)$ with and without final state interaction (solid and dashed lines, respectively). Note that due to a final state interaction, the two-magnon peak gets sharper, becomes more symmetric and shifts to a lower frequency. Bottom panel: 2D constant energy contours for the total energy of two magnons $\Omega(k + q_0/2) + \Omega(-k + q_0/2)$. The extended van-Hove singularity is at $\Omega(k + q_0/2) + \Omega(-k + q_0/2) = 2\sqrt{3}J$.

Our results for the full $R(q, \omega)$ partly agree and partly disagree with the experimental data for the inelastic resonance X-ray scattering of antiferromagnetic parent compounds La_2CuO_4 and Nd_2CuO_4 [10]. On one hand, the position *and* the profile of the peak fully agrees with our $R(q, \omega)$. Namely, the largest peak is at $q = q_0$, and it moves to smaller frequency and broadens on deviations from q_0 . On the other hand, we found, in agreement with [16] that due to final state interaction, the peak in $R(q_0, \omega)$ shifts down to $1.2E_{max} = 2.4J \sim 340meV$. This frequency is smaller than the experimental peak

frequency of $0.5eV \approx 3.6J$, which is close to the peak position at q_0 in the absence of the final state interaction. The peak shifts to a higher frequency if we include quantum corrections to the magnon dispersion [17], neglected in our analysis. Another possible explanation of the discrepancy may be that the RPA-type analysis of magnon-magnon interaction overestimates the effect of the final state interaction. For c -axis polarization of light, as in [10], the final state interaction involves the exchange between layers and generally should lead to a smaller down-shift of the peak position at $(0, \pi)$ from that for non-interacting magnons [18]. On the other hand, we didn't find the sharpest peak at $(0, \pi)$ for non-interacting magnons, e.g., in B_{1g} geometry, the peak at $(0, 0)$ is the sharpest. Magnon-magnon interaction substantially reduces this last peak, and the one at $(0, \pi)$ becomes the largest. However, this only happens if magnon-magnon

interaction is strong enough.

To summarize, we analyzed the profile of the X-ray scattering intensity $R(q, \omega)$ at finite q in a 2D Heisenberg antiferromagnet. Previous Raman scattering studies at $q = 0$ identified the two-magnon peak in B_{1g} geometry. We found that the B_{1g} peak slightly disperses downwards at a finite q , and its intensity increases, reaching its maximum at $q = q_0 = (0, \pi)$ and symmetry related points. Simultaneously, at a finite q , the intensity in A_{1g} geometry also becomes non-zero, and the A_{1g} Raman profile displays a two-magnon peak which disperses to larger frequencies with increasing q and reaches its highest intensity at q_0 . We found that the profile of $R(q_0, \omega)$ is equivalent in A_{1g} and B_{1g} geometries.

We thank G. Blumberg for useful conversations, constructive criticism, and for sharing Ref. [10] with us. The research was supported by NSF DMR 0240238.

-
- [1] A. Gozar, G. Blumberg, B. S. Dennis, B. S. Shastry, N. Motoyama, H. Eisaki, and S. Uchida, Phys. Rev. Lett. **87**, 197202 (2001); G. Blumberg, P. Abbamonte, M. V. Klein, W. C. Lee, D. M. Ginsberg, L. L. Miller, and A. Zibold, Phys. Rev. B **53**, R11930 (1996); R. R. P. Singh, P. A. Fleury, K. B. Lyons, and P. E. Sulewski, Phys. Rev. Lett. **62**, 2736 (1989); R.R.P. Singh, Comments Condens. Matter Physics **15**, 241 (1991).
- [2] R. Coldea, S. M. Hayden, G. Aeppli, T. G. Perring, C. D. Frost, T. E. Mason, S. -W. Cheong, and Z. Fisk, Phys. Rev. Lett. **86**, 5377 (2001).
- [3] P. A. Fleury and R. Loudon, Phys. Rev. **166**, 514 (1968).
- [4] W. Hayes and R. Loudon, *Scattering of light by crystals* (John Wiley and Sons, New York, 1978) p. 15 and p.121.
- [5] A. V. Chubukov and D. M. Frenkel, Phys. Rev. B **52**, 9760 (1995).
- [6] B. S. Shastry and B. I. Shraiman, Phys. Rev. Lett. **65**, 1068 (1990); Int. J. Mod. Phys. B **5**, 365 (1991).
- [7] T. P. Devereaux and A. P. Kampf, Int. J. Mod. Phys. B **11**, 2093 (1997).
- [8] A. Katani and S. Shin, Rev. Mod. Phys **73**, 203 (1991).
- [9] J. van den Brink and M. van Veenendaal, J. Phys. Chem. Solids **66**, 2145 (2005).
- [10] J. P. Hill, G. Blumberg, Young-June Kim, D. Ellis, S. Wakimoto, R.J Birgeneau, S. Komiya, Y. Ando, D. Casa, and T. Gog, *Observation of a new mid-IR mode in $La_{2-x}Sr_xCuO_4$* , preprint.
- [11] N. A. Dyson, *X-Rays in atomic and nuclear physics* - 2nd ed. (Cambridge University Press, Cambridge, 1990) p. 97.
- [12] A.V. Chubukov and K. A. Musaelian, Phys. Rev. B **50**, 6238 (1994).
- [13] P.M. Platzman and E.D. Isaaks, Phys. Rev. B **57**, 11107 (1988).
- [14] C. M. Canali and S. M. Girvin, Phys. Rev. B **45**, 7127 (1995).
- [15] A. Singh and Z. Tesanovic, Phys. Rev. B **41**, 11457 (1990).
- [16] J. Lorenzana and G.A. Sawatzky, Phys. Rev. Lett, **74**, 1867 (1995).
- [17] T. Oguchi, Phys. Rev. **117**, 117 (1960).
- [18] G. Blumberg, private communication.